THE ASTROPHYSICAL JOURNAL, 554:578–586, 2001 June 10

THE *r*-PROCESS IN NEUTRINO-DRIVEN WINDS FROM NASCENT, "COMPACT" NEUTRON STARS OF CORE-COLLAPSE SUPERNOVAE

SHINYA WANAJO,[1,2] TOSHITAKA KAJINO,[2,3,4] GRANT J. MATHEWS,[2,5] AND KAORI OTSUKI[2]

Received 2000 October 21; accepted 2001 February 15

ABSTRACT

We present calculations of *r*-process nucleosynthesis in neutrino-driven winds from the nascent neutron stars of core-collapse supernovae. A full dynamical reaction network for both the α-rich freezeout and the subsequent *r*-process is employed. The physical properties of the neutrino-heated ejecta are deduced from a general relativistic model in which spherical symmetry and steady flow are assumed. Our results suggest that proto–neutron stars with a large compaction ratio provide the most robust physical conditions for the *r*-process. The third peak of the *r*-process is well reproduced in the winds from these "compact" proto–neutron stars even for a moderate entropy, $\sim 100N_A k$–$200N_A k$, and a neutrino luminosity as high as $\sim 10^{52}$ ergs s^{-1}. This is due to the short dynamical timescale of material in the wind. As a result, the overproduction of nuclei with $A \lesssim 120$ is diminished (although some overproduction of nuclei with $A \approx 90$ is still evident). The abundances of the *r*-process elements per event is significantly higher than in previous studies. The total integrated nucleosynthesis yields are in good agreement with the solar *r*-process abundance pattern. Our results have confirmed that the neutrino-driven wind scenario is still a promising site in which to form the solar *r*-process abundances. However, our best results seem to imply both a rather soft neutron-star equation of state and a massive proto–neutron star that is difficult to achieve with standard core-collapse models. We propose that the most favorable conditions perhaps require that a massive supernova progenitor forms a massive proto–neutron star by accretion after a failed initial neutrino burst.

Subject headings: nuclear reactions, nucleosynthesis, abundances — stars: abundances — stars: mass loss — stars: neutron — supernovae: general

1. INTRODUCTION

The *r*-process accounts for the origin of about half of the abundances of elements heavier than iron. The other half mostly come from the *s*-process. Nevertheless, the astrophysical site for the *r*-process has not yet been unambiguously identified. Among the large number of proposed candidates, the neutrino-heated ejecta from a nascent neutron star (hereafter "neutrino-driven wind") has been suggested (Woosley & Hoffman 1992; Meyer et al. 1992) as perhaps the most promising site. Woosley et al. (1994) demonstrated that the solar *r*-process abundances were well reproduced as material was ablated from the proto–neutron star in neutrino-driven winds. There are, however, a few serious problems in their numerical results. First, elements with $A \sim 90$ were significantly overproduced by over a factor of 100. Second, the requisite high entropy ($\gtrsim 400N_A k$) in their supernova simulations has not been duplicated by other independent theoretical studies (Witti, Janka, & Takahashi 1994; Takahashi, Witti, & Janka 1994; Qian & Woosley 1996). On the other hand, other viable sites have been demonstrated to also naturally reproduce the solar *r*-process abundance pattern. For example, it has been shown that neutron-star mergers can naturally reproduce the abundances of nuclei with $A \gtrsim 130$ (Freiburghaus, Rosswog, & Thielemann 1999). Collapsing O-Ne-Mg cores resulting from progenitor stars of ~ 8–$10\ M_\odot$ have also been suggested (Wheeler, Cowan, & Hillebrandt 1998) to be a promising site for the *r*-process.

In contrast to the above difficulties in the theoretical studies of the neutrino-driven wind scenario, observational data seem to confirm that Type II supernovae are indeed the site for the production of *r*-process elements. For example, spectroscopic studies of metal-poor halo stars indicate very early enrichment of *r*-process elements consistent with production in massive stars (Sneden et al. 1996, 1998; Ryan, Norris, & Beers 1996). Using a chemical evolution model, Ishimaru & Wanajo (1999) have furthermore demonstrated that the large dispersion of the *r*-process element europium in metal-poor halo stars is also reproduced if the *r*-process originates from Type II supernovae (see also Tsujimoto, Shigeyama, & Yoshii 2000; Qian 2000).

As one way to fix the schematic wind models, it has been suggested that general relativistic effects increase the entropy and reduce the dynamical timescale of neutrino-driven wind models. Using semianalytic studies for spherically symmetric, steady flow of neutrino-heated ejecta, Qian & Woosley (1996) showed that the inclusion of a first post-Newtonian correction to the gravitational force equation increased the entropy by $\sim 60\%$ and reduced the timescale by a factor of ~ 2. Cardall & Fuller (1997) further developed this argument by considering a fully general relativistic treatment. They considered a wide range of neutron-star compaction ratios (ratio of the gravitational mass to the neutron star radius in Schwarzschild coordinates). They showed that a more compact neutron star leads to significantly higher entropy and a shorter dynamical timescale in

[1] Department of Physics, Sophia University, 7-1 Kioi-cho, Chiyoda-ku, Tokyo 102-8554, Japan; wanajo@sophia.ac.jp.
[2] Division of Theoretical Astrophysics, National Astronomical Observatory, 2-21-1 Osawa, Mitaka, Tokyo 181-8588, Japan; kajino@nao.ac.jp, gmathews@nd.ed, otsuki@th.nao.ac.jp.
[3] Department of Astronomy, University of Tokyo 7-3-1 Hongo, Bunkyo, Tokyo 113-0033, Japan.
[4] Department of Astronomical Science, The Graduate University for Advanced Studies, 2-21-1 Osawa, Mitaka, Tokyo 181-8588, Japan.
[5] Center for Astrophysics, Department of Physics, University of Notre Dame, Notre Dame, IN 46556.

the wind. In their study, however, the sensitivity to the neutron star mass and neutrino luminosity were not considered.

Otsuki et al. (2000, hereafter Paper I) studied physical conditions of neutrino winds in a manner similar to that of Cardall & Fuller (1997), for wide ranges of the neutron star masses and the neutrino luminosities. They suggested that high entropy and short dynamical timescales were obtained for a massive neutron star and a high-neutrino luminosity. However, the radii of the neutron stars were fixed to be 10 km in their study. Moreover, these studies did not perform calculations of realistic r-process nucleosynthesis except for one specific case of a neutron star mass ($= 2\ M_\odot$) and a neutrino luminosity ($L_{\nu_e} = 10^{52}$ ergs s^{-1}) in Paper I.

The purpose of the present study is therefore to examine more quantitatively the r-process in neutrino-driven winds utilizing a fully implicit reaction network of over 3000 isotopes. Trajectories of thermodynamic quantities for material in the winds are derived for various combinations of three parameters: the neutron star mass, radius, and neutrino luminosity. The semianalytic, general relativistic model developed in Paper I is adopted to describe material in the neutrino-driven wind.

The paper is organized as follows: In § 2, the dependences of the entropy and the dynamical timescale on the neutron star mass, compaction ratio, and neutrino luminosity are discussed. In § 3, the r-process nucleosynthesis is performed using the neutrino-driven wind trajectories obtained in § 2. The yields for various neutrino luminosities are mass-integrated by assuming an exponential time evolution for the neutrino luminosity. These are compared to the solar r-process abundances. The implications of this study are discussed in § 4.

2. NEUTRINO-DRIVEN WINDS

The models of neutrino-driven winds used in this work were developed in detail in Paper I. We briefly describe the models here and point out some improvements that have been added. The system is treated as time-stationary and spherically symmetric. The physical variables in the neutrino wind are then functions of the radius r only. The ejected mass $M_{\rm ej}$ by neutrino heating is assumed to be negligible compared to the mass of the neutron star M. Therefore, the gravitational field in which the neutrino-heated matter moves can be treated as a fixed background Schwarzschild metric. The equations of baryon, momentum, and mass-energy conservation then become

$$\dot{M} = 4\pi r^2 \rho u\ , \tag{1}$$

$$u\frac{du}{dr} = -\frac{1 + (u/c)^2 - 2GM/c^2 r}{\rho(1 + \epsilon/c^2) + P/c^2}\frac{dP}{dr} - \frac{GM}{r^2}\ , \tag{2}$$

$$\dot{q} = u\left(\frac{d\epsilon}{dr} - \frac{P}{\rho^2}\frac{d\rho}{dr}\right), \tag{3}$$

where $\dot{M}$ is the mass ejection rate from the surface of the neutron star, $\dot{q}$ is the heating rate, ρ is the mass density, P is the pressure, and ϵ is the specific internal energy (Shapiro & Teukolsky 1983). The velocity u is related to the proper velocity of the matter v as measured by a local, stationary observer by

$$v = \left[1 + \left(\frac{u}{c}\right)^2 - \frac{2GM}{c^2 r}\right]^{-1/2} u\ . \tag{4}$$

The source term $\dot{q}$ includes both heating and cooling by neutrino interactions. Heating is due to neutrino and antineutrino captures by free nucleons, neutrino scattering on electrons and positrons, and neutrino-antineutrino pair annihilation into electron-positron pairs. The redshift of neutrino energies and bending of the neutrino trajectories by general relativity are explicitly taken into account. Cooling is due to electron and positron capture by free nucleons, and annihilation of electron-positron pairs into neutrino-antineutrino pairs. For the latter, the more accurate table of Itoh et al. (1996) is utilized rather than equation (15) in Paper I. All other neutrino heating and cooling rates are taken from Paper I.

The neutrino luminosities L_ν of all flavors are assumed to be equal, and the rms average neutrino energies are taken to be 12, 22, and 34 MeV, for electron, antielectron, and the other flavors of neutrinos, respectively. The temperature at the surface of the neutron star is determined so that heating and cooling by neutrino interactions are in equilibrium. The surface of the neutron star is arbitrarily defined as the point at which density has dropped to $\rho = 10^{10}$ g cm^{-3}. The equation of state for the electron and positron gas includes not only the relativistic pairs as in Paper I but also the partially relativistic pairs, which are important during the α-process. Once M, R, and L_ν are specified along with the boundary condition $\dot{M}$, we obtain numerically the velocity and thermodynamic quantities of the neutrino-driven wind as functions of r.

In Paper I, $\dot{M}$ for each neutrino-driven wind was fixed such that the temperature at $r = 10{,}000$ km was 0.1 MeV. However, in that case no physical solution exists for $L_\nu \gtrsim 10^{52}$ ergs s^{-1} because the temperature does not cool to 0.1 MeV before the wind reaches $r = 10{,}000$ km for any physical solutions. Note that equations (1)–(3) have no physical solution for $\dot{M} > \dot{M}_{\rm max}$. In order to avoid this discontinuity, we instead adopt $\dot{M} = \dot{M}_{\rm max}$, which allows for a supersonic wind. The advantage is that the wind solution exists for any L_ν, even larger than 10^{52} ergs s^{-1}.

We evaluate the key parameters for the r-process, i.e., entropy and dynamical timescale, as a function of $\dot{M}_{\rm max}$ instead of arbitrary $\dot{M}$ for each L_ν. When nucleosynthesis calculations are performed, we actually take $\dot{M}$ to be slightly smaller than $\dot{M}_{\rm max}$ to obtain solutions for subsonic winds, as discussed below. As initial conditions, we make the reasonable assumptions that the electron fraction Y_e is set to 0.5 and that no α-particles or heavy elements have yet formed.

In this study, we explore three specific models of the neutrino-driven winds based upon combinations of two parameters M and R. The models given in Table 1 correspond to model A: (M, R) = (1.4 $M_\odot$,10 km); model B: (M, R) = (1.4 $M_\odot$, 7 km); and model C: (M, R) = (2.0 $M_\odot$, 10 km). The difference between models A and B is the compaction

TABLE 1

MODEL PARAMETERS

	MODEL		
PARAMETER	A	B	C
$M/M_\odot$	1.4	1.4	2.0
R (km)	10	7	10
GM/c^2R.....	0.21	0.30	0.30

ratio GM/c^2R, while neutron star mass is the same. On the other hand, effects of general relativity are manifest through the compaction ratio. Models B and C therefore involve different masses and radii, while the compaction ratio is the same. The compaction ratio for models B and C is rather large, ~ 0.3. However, this value is still consistent with relatively soft equations of state for high-density matter or as a metastable state prior to collapse to a black hole (Brown & Bethe 1994; Baumgarte et al. 1996). Note that the case of a smaller compaction ratio $\lesssim 0.2$ is omitted in this study, where r-processing may not be possible (Cardall & Fuller 1997).

Figure 1*a* shows the mass ejection rate $\dot{M}_{\rm max}$, Figure 1*b*, the entropy per baryon S/k at $T = 0.5$ MeV, and Figure 1*c*, the dynamical timescale τ measured as the time for material to cool from $T = 0.5$ to 0.2 MeV, as a function of L_ν for supersonic winds. The mass ejection rate is the maximum value for physical solutions of the winds. The dot-dashed, dashed, and thick solid lines, respectively, denote models A, B, and C. As can be seen in Figure 1, for larger L_ν, $\dot{M}_{\rm max}$ and S take larger and smaller values, respectively. A similar trend in entropy can be seen in τ. However, the timescale saturates at L_ν approximately a few times 10^{52} ergs s^{-1}. This can be traced to the smaller transonic radii $r_{\rm c}$ and higher initial temperature for higher neutrino luminosities. The temperature gradient is steeper when r is closer to the neutron star surface while being approximately constant for $r > r_{\rm c}$ (Paper I). Thus, the temperature decreases more slowly for $r > r_{\rm c}$ than for $r < r_{\rm c}$. For higher luminosity cases $\gtrsim 10^{52}$ ergs s^{-1}, the winds pass $r_{\rm c}$ with $T > 0.2$ MeV. As a result, the dynamical timescale does not decrease for higher luminosities.

The r-process favors higher entropy and shorter dynamical timescale. Thus, a robust r-process is difficult to obtain once the neutrino luminosity is higher than a few times 10^{52} ergs s^{-1}. Comparing the results of models A and B (or models A and C), we find that more "compact" proto–neutron stars eject less material and obtain significantly higher entropies and shorter dynamical timescales. This is in good agreement with the results of Cardall & Fuller (1997). Clearly, the more "compact" neutron star models (B and C) will obtain more favorable physical conditions for the r-process.

On the other hand, comparing the results of models B and C, which are at the same compaction ratio, we see that a more massive (or smaller radius) proto–neutron star ejects slightly less material and provides higher entropy but involves a larger dynamical timescale. These can be explained by the relations $\dot{M} \propto R^{5/3}M^{-2}$, $S \propto R^{-2/3}M$, and $\tau \propto RM$ for fixed energy and neutrino luminosity (Qian & Woosley 1996) in the Newtonian limit. On the basis of these results alone it is difficult to judge which of the models B or C is more favorable for the r-process. Differences of the nucleosynthesis results between these models are to be discussed in § 3.

Figure 1 also shows the results of the numerical simulation of the winds from Sumiyoshi et al. (2000) for $(M, R) = (1.4\ M_\odot, 10\ \text{km})$ and $(2.0\ M_\odot, 10\ \text{km})$, respectively. These are denoted by filled squares and circles. Open squares and circles show the results of Qian & Woosley (1996) calculated with post-Newtonian corrections for the same parameter sets of (M, R). Our results for $\dot{M}$, S, and τ are in good agreement with theirs. Ultimately, mass ejection rates must be determined by a detailed hydrodynamic simulation of a proto–neutron star with neutrino transport being taken into consideration. Nevertheless, our mass ejection rates, entropies, and dynamical timescales are in good agreement with those of Sumiyoshi et al. (2000), who calculated steady-flow neutrino-driven winds with the use of a one-dimensional hydrodynamic code including neutrino heating and cooling processes. Thus, we conclude that the true mass ejection rates are probably close to the supersonic winds obtained here.

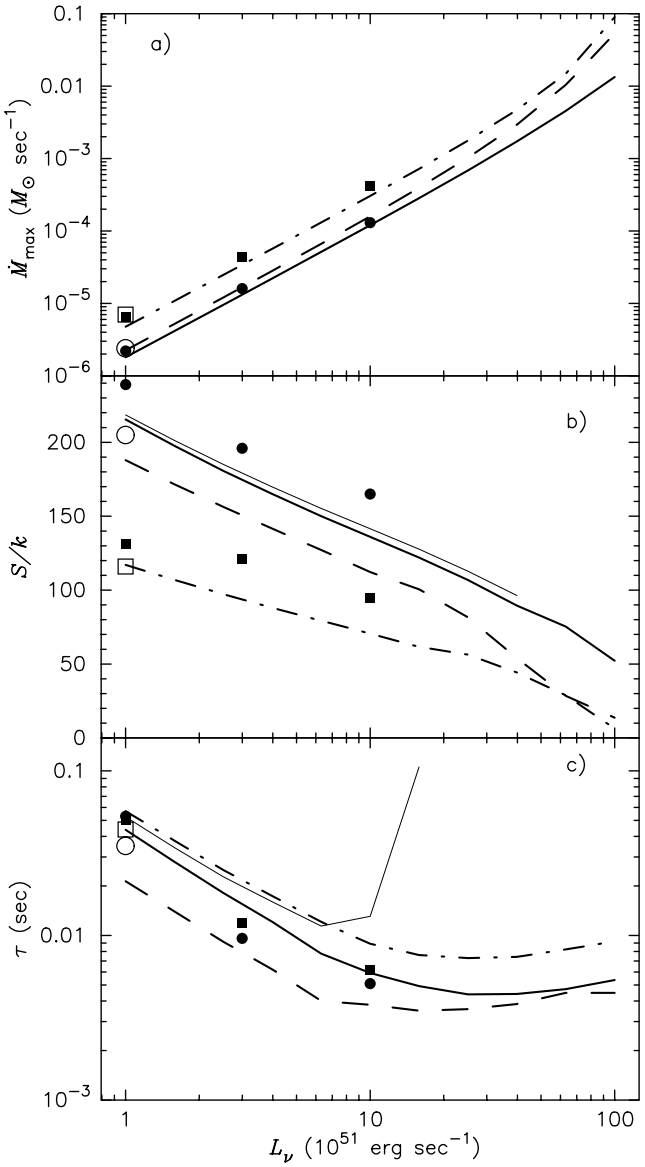

FIG. 1.—(*a*) Maximum mass ejection rates, (*b*) entropy per baryon, and (*c*) dynamical timescales measured as the time for material to cool from $T = 0.5$ to 0.2 MeV for models A (*dot-dashed line*), B (*dashed line*), and C (*thick-solid line*), as functions of L_ν for the supersonic winds. The thin solid lines in panels (*b*) and (*c*) are for the subsonic wind with $\dot{M} = 0.995\dot{M}_{\rm max}$ for model C (see text). Also denoted are the results from Sumiyoshi et al. (2000, *filled squares and circles*) and Qian & Woosley (1996, *open squares and circles*). In both cases, the squares and circles are the results with the same model parameters $M/M_\odot$ and R as the models A and B, respectively.

Without imposing an outer boundary, however, the temperature and density diminish too quickly in the supersonic winds. This is not favorable for the r-process. Therefore, a

slightly smaller mass ejection rate, $0.995\dot{M}_{\max}$, is adopted for application to r-process calculations in § 3. The advantage of this reduction is that the temperature and density fall off slowly during the r-process ($T_9 \lesssim 2.5$) in these subsonic winds, ensuring enough time for the nucleosynthesis of heavy elements to proceed. This situation resembles the wind with an outer boundary, as if a supersonic wind interacts with a wall shock to sustain the temperature and density suitable for the r-process. The entropy per baryon and the dynamical timescale for model C with this $\dot{M}$ are displayed in Figures 1*b* and 1*c* by thin solid lines. This small reduction of $\dot{M}$ increases the entropy per baryon only about a few percent. The dynamical timescale also increases by a factor of $\lesssim 2$ for $L_\nu \leq 10^{52}$ ergs s^{-1}. For $L_\nu > 10^{52}$ ergs s^{-1}, however, the dynamical timescale increases drastically. This is because the winds pass r_c with $T > 0.2$ MeV for higher luminosity cases. Furthermore, the velocity and the radial gradient in temperature decrease significantly after the wind crosses r_c for a subsonic wind (Paper I). This situation that the dynamical timescale becomes significantly longer at an early stage is similar to the results of previous detailed hydrodynamic simulations (Woosley et al. 1994; Witti et al. 1994). Obviously, the r-process would not take place in the winds for $L_\nu > 10^{52}$ ergs s^{-1} owing to the too long dynamical timescales, as to be confirmed by nucleosynthesis calculations in the next section. Note that the entropy per baryon for $L_\nu > 10^{52.6}$ ergs s^{-1} and the dynamical timescale for $L_\nu > 10^{52.2}$ ergs s^{-1} are not displayed in Figures 1*a* and 1*b* since the temperature at 10^4 km, where the calculation is stopped, is higher than 0.5 and 0.2 MeV, respectively.

3. THE r-PROCESS

Nucleosynthesis yields from the r-process were calculated for the three neutrino-driven wind models discussed in § 2. We used a fully implicit nuclear reaction network for both the α-rich freezeout and the subsequent r-process. The network consists of over 3000 isotopes all the way from neutron and proton up to the plutonium isotopes. We include all relevant reactions, i.e., (n, γ), (p, γ), (α, γ), (p, n), (α, p), (α, n), and their inverse. Reaction rates were taken from F. K. Thielemann (1995, private communication) for nuclei with $Z \leq 46$ and from Cowan, Thielemann, & Truran (1991) for those with $Z \geq 47$. Weak interactions such as β-decay, β-delayed neutron emission, electron capture, and the capture of electron and antielectron neutrinos on free nucleons were also included. These neutrino capture processes are of importance as they reduce the number of free neutrons by the "α-effect" (Meyer, McLaughlin, & Fuller 1998). Note that fission reactions are not included.

Nucleosynthesis calculations were carried out in nine trajectories with neutrino luminosities between $\log L_\nu$(ergs s^{-1}) = 52.6 and 51.0 in intervals of 0.2 dex. The mass ejection rates were taken to be $0.995\dot{M}_{\max}$ as described in § 2. Each calculation started when the temperature decreased to $T_9 = 9$ (where $T_9 \equiv T/10^9$ K). At this point the nuclear statistical equilibrium (NSE) consists mostly of free nucleons. The initial mass fractions of neutrons and protons were therefore given by NSE plus charge neutrality: $X_n = 1 - Y_e$ and $X_p = Y_e$, respectively. The initial electron fraction Y_e was set to be 0.40, which is near the lower bound for neutrino-heated ejecta from the models of Woosley et al. (1994). This approximation is adequate for our study, although ultimately the initial electron fraction should be determined by the detailed balance of the energy and luminosity between electron and antielectron neutrinos with a hydrodynamic study.

Figure 2 illustrates the final abundance of each trajectory for model C as a function of mass number. It is found that the trajectories with $\log L_\nu$(ergs s^{-1}) ≤ 52.0 (Figs. 2*d*–2*i*) result in a robust r-process. This is due to the sufficiently high entropies, $S \gtrsim 140k$, and short dynamical timescales, $\tau \lesssim 30$ ms (Fig. 1). Figure 3 shows the neutron-to-seed ratio $Y_n/Y_{\rm seed}$ (*solid line*), the mass fraction of seed nuclei $X_{\rm seed}$ (*dashed line*), and the electron fraction Y_e (*dot-dashed line*) at $T_9 = 2.5$, which is approximately the temperature at the beginning of the r-process phase. Here "seed" refers to all nuclei with $A \geq 12$. The final mass fraction of r-process elements ($A \geq 100$) X_r is also shown by the dotted line. As can be seen in Figure 3, the neutron-to-seed ratio reaches the maximum ~ 160 at $\log L_\nu$(ergs s^{-1}) = 51.8. As a result, for the corresponding trajectory, the third abundance peak and the heavier nuclei are prominent (Fig. 2*e*). However, the total abundance of r-process nuclei produced from this trajectory is small. This is because the mass fraction of seed nuclei obtains the minimum value at this luminosity, as can be seen in Figure 3. Note that X_r is smaller for $L_\nu > 10^{52}$ ergs s^{-1} despite higher $X_{\rm seed}$ owing to the smaller neutron-to-seed ratio. For lower luminosities $\log L_\nu$(ergs s^{-1}) $\leq$ 51.6, β-delayed neutron emission smooths the abundance pattern as seen in Figure 2 because of the longer dynamical timescales (Fig. 1).

As anticipated in § 2, trajectories for $\log L_\nu \geq 52.2$ (Figs. 2*a*–2*c*) do not contribute significantly to the r-process because of the too long dynamical timescales (Fig. 1*c*). Neutrino capture on free nucleons somewhat increases the electron fraction to $Y_e \sim 0.42$–0.43 at $T_9 = 2.5$ by the α-effect (Meyer et al. 1998) as seen in Figure 3 (*dot-dashed line*). Thus, it is important to include the neutrino capture reactions in order to correctly calculate the resulting r-process nucleosynthesis. This effect is not, however, as serious as that suggested by Meyer et al. (1998) in the present r-process conditions. The reason is that the dynamical timescales in our models $\tau \lesssim 30$ ms are sufficiently shorter than the neutrino interaction lifetime for the neutrino luminosities considered. The dynamical timescale of Meyer et al. (1998) was fixed at a value as large as $\tau = 0.3$ s.

In order to compare the nucleosynthesis results of each model with the solar-system r-process abundances, the yields were integrated over the mass-weighted time history in the following manner. The time evolution of the neutrino luminosity is approximately given by

$$L_\nu = L_{\nu 0} \exp\left(\frac{-t}{\tau_\nu}\right), \tag{5}$$

where $L_{\nu 0}$ is the initial neutrino luminosity at the neutrino sphere and τ_ν is the cooling timescale. We take $L_{\nu 0}$ to be $\approx 4 \times 10^{52}$ ergs s^{-1} ($\log L_{\nu 0} = 52.6$) from Woosley et al. (1994). In principle, $L_{\nu 0}$ depends on the radius of neutrino sphere and should be corrected for the gravitational redshift effect on neutrino energy. However, the present approximation is adequate for our purposes as neutrino-driven winds with $L_\nu \gtrsim 4 \times 10^{52}$ ergs s^{-1} do not substantially contribute to the r-process yields. The cooling timescale τ_ν is set equal to 1.25 s so that the total time-integrated neutrino energy becomes 3×10^{53} ergs. With this τ_ν, the Figures 2*a*–2*i* correspond to time slices at 0, 0.6, 1.2, 1.7, 2.3, 2.9, 3.5, 4.0, and 4.6 s, respectively.

We integrate the mass-weighted r-process yields assuming that the trajectories can be described at each time

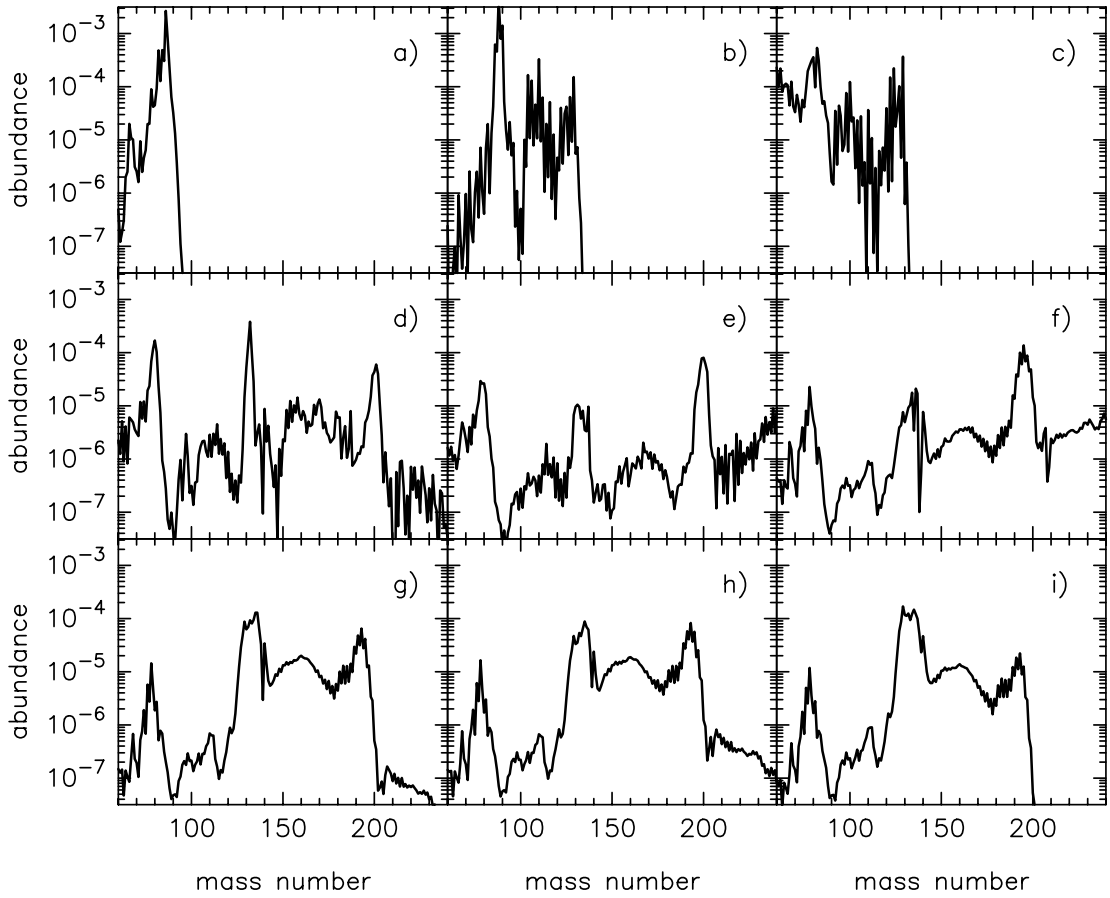

FIG. 2.—Final abundances in model C as a function of atomic mass number for log L_ν (ergs s^{-1}) = (*a*) 52.6, (*b*) 52.4, (*c*) 52.2, (*d*) 52.0, (*e*) 51.8, (*f*) 51.6, (*g*) 51.4, (*h*) 51.2, and (*i*) 51.0.

by steady flow corresponding to the neutrino luminosity and neutron star radius at that time,

$$Y_i = \frac{1}{M_{\rm ej}} \int Y_i(t)\dot{M}(t)dt \ , \tag{6}$$

where

$$M_{\rm ej} = \int \dot{M}(t)dt \tag{7}$$

is the total mass ejected from the neutron star.

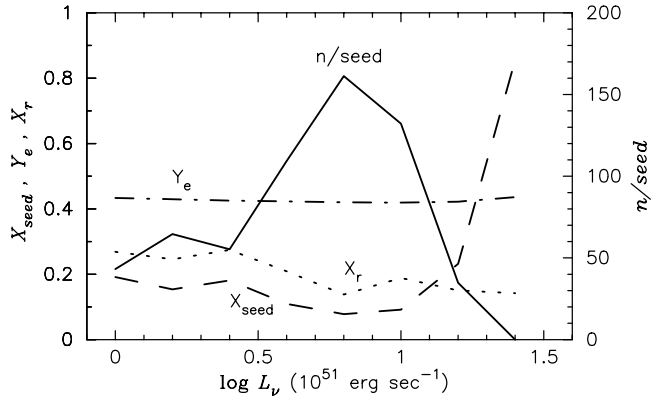

FIG. 3.—Neutron-to-seed ratio (*solid line*), the mass fraction of seed nuclei (*dashed line*), and the electron fraction (*dot-dashed line*) at $T_9 = 2.5$. The final mass fraction of *r*-process elements ($A \geq 100$) is also denoted by the dotted line.

Obviously, our assumption of steady flow for each trajectory is oversimplified. However, the thermal properties of material in the neutrino-heated wind are mostly determined near the surface of the neutron star $\lesssim$30 km, where the equilibration time ($\lesssim$0.1 s) is shorter than the neutrino luminosity timescale τ_ν ($\sim$1 s). In addition, during the relaxation of the neutron star radius $\sim$2 s, the neutrino luminosity is so high, $L_\nu \gtrsim 10^{52}$ ergs s^{-1}, that few *r*-process elements are synthesized. Hence, the assumptions of steady flow for each neutrino luminosity and a fixed neutron star radius are probably reasonable.

In Figure 4, the integrated yields for models A, B, and C are compared with the solar system *r*-process abundances (Käppeler, Beer, & Wisshak 1989). In models B and C the solar *r*-process abundances are normalized to the third peak. For model A the second peak is used for normalization. Comparison of the three results suggests that the "compaction" of the proto–neutron star is essential to reproduce the pattern of the solar *r*-process abundances. Indeed, the abundance pattern for elements with $A \gtrsim 120$ in models B and C are in excellent agreement with the scaled solar *r*-abundances, while only a weak *r*-process occurred in model A.

In all three models there is about a factor of 10 overproduction of nuclei with $A \lesssim 120$. For $A \approx 90$ in particular, there is a prominent peak as also seen in previous studies (Freiburghaus et al. 1999). In the present models, however, the overproduction is about a factor of 10 smaller than that of Woosley et al. (1994). Moreover, if the abun-

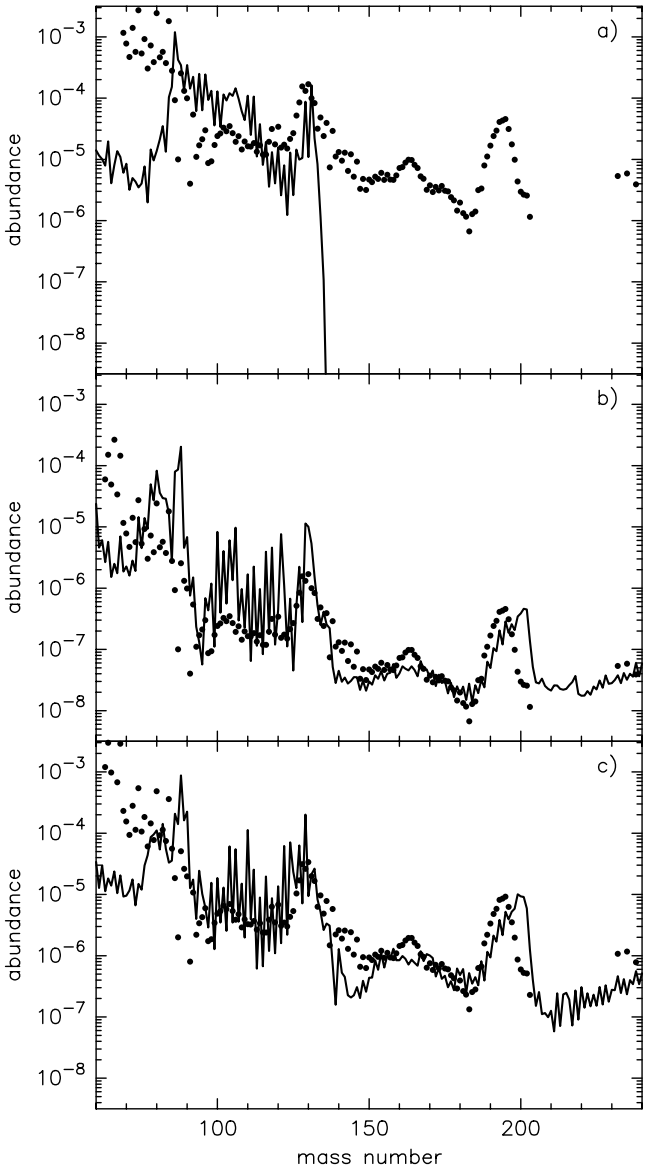

FIG. 4.—Mass-weighted integrated yields for models (*a*) A, (*b*) B, and (*c*) C as functions of mass number (*lines*). Also denoted are the scaled solar *r*-abundances (*filled circles*).

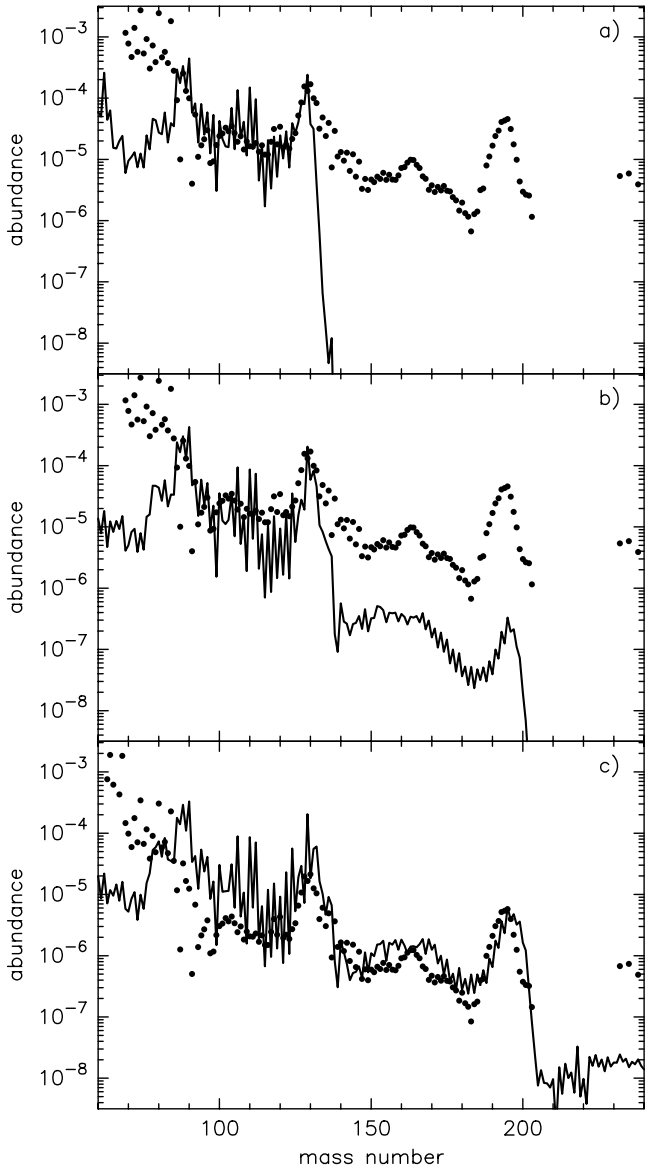

FIG. 5.—Same as Fig. 4, but for (*a*) (M, R) = (1.7 $M_\odot$,10 km), (*b*) (1.8 $M_\odot$,10 km), and (*c*) (1.9 $M_\odot$,10 km).

dances of $A \sim 100$–130 were smoothed, they would agree reasonably well with the solar *r*-pattern.

The good agreement in models B and C is a consequence of the robust *r*-process that starts at the early phase (~ 2 s) of the neutrino-driven wind. At this time L_ν is still as high as $\sim 10^{52}$ ergs s^{-1}, and the integrated yields are dominated by the matter ejected there. This is in contrast to the result of Woosley et al. (1994), in which the *r*-process occurs only during the late phase of the neutrino-driven wind (~ 10 s), where the mass ejection rate has already significantly declined.

TABLE 2

TOTAL EJECTED MASS

EJECTED MASS	MODEL			
	A	B	C	W94[a]
$M_{ej}/M_\odot$	2.9×10^{-3}	1.7×10^{-3}	1.1×10^{-3}	3.2×10^{-2}
$M_{ej,r}/M_\odot$	5.3×10^{-4}	2.0×10^{-5}	1.4×10^{-4}	5.8×10^{-5}[b]

[a] Woosley et al. 1994.

[b] Abundances produced in the last 16 trajectories.

In Table 2, the total ejected mass M_{ej} and mass of *r*-process ($A \geq 100$) elements $M_{ej,r}$ for each model are compared to those of Woosley et al. (1994). Note that $M_{ej,r}$ in the W94 column is the sum of the last 16 trajectories in Woosley et al. (1994), whose pattern was in excellent agreement with the solar *r*-abundances. The ejected *r*-process mass in model C is about a factor of 2 larger than that of Woosley et al. (1994) owing to production of *r*-nuclei in early times when $\dot{M}$ is high. It is interesting to note that the total ejected masses of all models are smaller than that of Woosley et al. (1994), while $\dot{M}$ is set to be nearly equal to the maximum value in this study. This is a consequence of our more compact neutron stars, which obtain smaller $\dot{M}$ as can be seen in Figure 1*a*. In particular, the radius of the neutron star in Woosley et al. (1994) is much larger than 10

km in the first few seconds, while those in this study are taken to be constant. In addition, $\dot{M}$ in Woosley et al. (1994) during the first ~ 1 s is significantly larger than expected for a steady state wind.

Comparing the three models in Table 2, we see that M_{ej} does not significantly change from model to model, being somewhat smaller in models with a deeper gravitational potential. As can be seen in Figure 4, however, the *r*-abundance pattern is substantially different among these models. Model A reproduces the first ($A \sim 80$) and second ($A \sim 130$) *r*-process peaks, but no elements with $A \gtrsim 130$ are synthesized. In contrast, the solar *r*-pattern, including all three *r*-process peaks, is well reproduced in the "compact" neutron star models B and C. This is a consequence of the significantly higher entropies $S \gtrsim 130 N_A k$ and shorter dynamical timescales $\tau \lesssim 30$ ms for these models.

Comparing the absolute yields in models B and C, we find that the neutrino-driven wind of a more massive proto–neutron star produces more *r*-process elements when the compaction ratio is the same. Indeed, the mass fraction of *r*-elements in model C is about a factor of 10 larger than that of model B. The reason is that the dynamical timescale in model B is shorter than in model C (cf. Fig. 1). In such fast winds, fewer seed nuclei are produced, although the neutron-to-seed ratio is high enough for a robust *r*-process (see also Hoffman, Woosley, & Qian 1997).

Let us discuss how sensitive these results are to the compaction ratio. We present in Figure 5 the mass-weighted integrated yields for three more cases: $(M, R) = (1.7\ M_\odot$, 10 km), (1.8 $M_\odot$, 10 km), and (1.9 $M_\odot$, 10 km). These correspond to compaction ratios of 0.25, 0.27, and 0.28, respectively. Interestingly, the pattern in the first model is not significantly different from that of model A. In fact, it is in slightly better agreement with the first and second solar *r*-process peaks but does not produce heavier elements (Fig. 5*a*). The second model produces a small amount of $A > 130$ elements, and the third one reasonably reproduces the solar *r*-pattern up to the third peak (Figs. 5*b* and 5*c*). These calculations indicate that the *r*-process strongly depends on the compaction ratio. A good fit is obtained only when the compaction ratio is $\gtrsim 0.28$.

4. DISCUSSIONS AND CONCLUSION

We have explored the *r*-process in neutrino-heated ejecta (neutrino-driven winds) from nascent neutron stars for various neutron star masses, radii, and neutrino luminosities. Our results suggest that proto–neutron stars with a large compaction ratio ($GM/c^2R \sim 0.3$; models B and C), where general relativistic effects are important, provide the best conditions for the *r*-process. Such compact proto–neutron stars lead to sufficiently high entropy $S \sim 100 N_A k$–$200 N_A k$ and short dynamical timescales $\tau \lesssim 30$ ms to produce an optimum neutron-to-seed ratio for material in the neutrino-driven winds. The total time-integrated yields from these models are in good agreement with the solar *r*-process abundance pattern especially for nuclei with $A \sim 120$–200. Our short dynamical timescale and assumed condition of steady-flow equilibrium for material in the winds lead to a good *r*-process even at early times when the neutrino luminosity is still high, $L_\nu \sim 10^{52}$ ergs s^{-1}. As a result, the overproduction of nuclei $A \lesssim 120$ is significantly reduced, compared to that of Woosley et al. (1994), although still being overproduced by a factor of ~ 10.

Our results also suggest that for models of the same compaction ratio, e.g., B and C, a higher neutron star mass yields more *r*-process material. This is due to the somewhat longer dynamical timescale for material ejected from high-mass neutron stars, which increases the amount of seed nuclei.

The implication of these two results is that an optimum *r*-process without overproduction of $A \sim 90$ nuclei may require both a well-developed bubble and a massive proto–neutron star while the *r*-process elements are synthesized. It should be noted that we presume that the bubble is already evacuated and a steady state wind developed for all neutrino luminosities. For the dynamical supernova model of Woosley et al. (1994), however, the proto–neutron star is still relaxing and the bubble slowly expanding during the first ~ 2 s. In model C of this study, the *r*-process starts at $L_\nu = 10^{52}$ ergs (Fig. 2), which corresponds to 1.7 s in equation (5). At $L_\nu \sim 10^{52}$ ergs; therefore, the entropy per baryon might be somewhat overestimated, although the dynamical timescale as a function of L_ν shows a similar trend to those of previous hydrodynamic studies (Fig. 1*c*). A detailed hydrodynamic study of the neutrino-induced explosion for a massive supernova progenitor will be eventually needed to confirm whether the early stage of the neutrino-driven winds from compact neutron stars is really the astrophysical site of the *r*-process.

Alternatively, this scenario might occur if the low-entropy material initially ejected from the supernova were to fall back onto the neutron star. This would produce the massive remnant. This epoch might then be followed by a second epoch of high neutrino flux into the previously evacuated bubble. This might occur, for example, if the proto–neutron star were to experience a late transition to strange matter and subsequent neutrino emission or a late softening and heating by kaon condensation (Thorsson, Prakash, & Lattimer 1994). For example, the softening of a proto–neutron star by kaon condensation is estimated to occur in a few to 10 s after core bounce (Keil & Janka 1995), which may be relevant to the *r*-process in this study. In either case, it is clear that these new results could suggest an interesting new twist to the supernova paradigm.

If these models for the *r*-process are correct, then our results could also pose a significant constraint on the equation of state for the neutron star remnant. A summary of the mass-radius relationship of some contemporary equations of state is shown in Figure 6. These are compared with the various models considered in this work. These representative equations of state include an example of a nonrelativistic nucleon potential model equation of state with both two-body and three-body terms (AV14 + UVII; Wiringa, Fiks, & Fabrocini 1988), as well as various relativistic mean field equations of state, including those based upon a relativistic Hartree ("G" in Fig. 6; Glendenning 1989; and "HV"; Glendenning 1985), Hartree-Fock ("HVF"; Weber & Weigel 1989) calculation, and those with strange-matter interiors ("SS1" and "SS2"; Glendenning & Weber 1992).

Model A with $M = 1.4\ M_\odot$ and $R = 10$ km is a typical neutron star mass and a typical radius for a nonrelativistic equation of state and several relativistic ones as well. However, it does not produce a good *r*-process in our simulations. Generating the observed abundance curve seems to

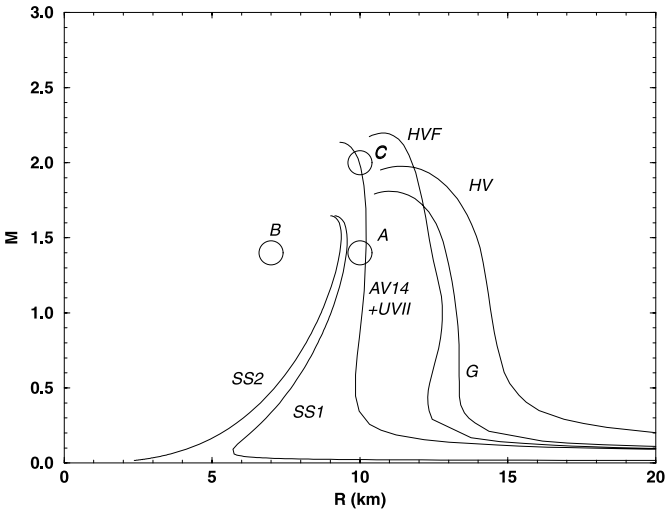

FIG. 6.—Comparison of the mass-radius relation (*lines*) for various equations of state with the models A, B, and C (*circles*) considered in this work. See text for an explanation of the various equations of state.

require a slightly more exotic paradigm. If we consider our best *r*-process model, i.e., model C with $M = 2.0\ M_\odot$ and $R = 10$ km, we see that many of the equations of state lead to such a remnant. In all cases, however, such a massive remnant is very close to or equal to the maximum mass allowed by the equation of state. If such a remnant is required to produce the *r*-process, then it seems that the *r*-process must occur for a remnant that has accreted to its maximum mass and is about to collapse to a black hole. This suggests another possible paradigm in which the *r*-process occurs in the previously evacuated bubble by neutrinos generated as the short-lived proto–neutron star begins its collapse to a black hole (see also Qian, Vogel, & Wasserburg 1998). This would perhaps require that the *r*-process occurs in a more massive progenitor star without leaving a neutron star remnant such as probably occurred in SN 1987A (Brown & Bethe 1994).

Although model B with $M = 1.4\ M_\odot$ and $R = 7$ km also gives a reasonable *r*-process abundance distribution, it is very difficult to form such a compact neutron star of this mass. Such lower mass high-compaction stars could perhaps form if a strange matter core develops as in SS1 and SS2 of Figure 6.

The results of this study are also of importance for the chemical evolution of the Galaxy. Ishimaru & Wanajo (1999) have suggested that the large dispersion of europium with respect to iron among metal-poor stars in the Galactic halo (Ryan et al. 1996; McWilliam 1997) can be reproduced if the *r*-process elements originate from stars of $\geq 30\ M_\odot$ or 8–10 $M_\odot$. Our results also imply that, for a given equation of state, a more massive proto–neutron star leads to a smaller compaction ratio and therefore more favorable conditions for the *r*-process. Furthermore, if the maximum mass of a proto–neutron star were as large as $\sim 2\ M_\odot$, the progenitor star is probably very massive. Such stars with $\geq 30\ M_\odot$ account for only $\sim 10\%$ of all supernova progenitors with a typical initial mass function. Nevertheless, the amount of *r*-process matter in model C is about a factor of 2 higher than that of Woosley et al. (1994) so that such a restriction to high-mass stars may be reasonable.

It should be noted that, even if neutrino-driven winds fail to reproduce the solar *r*-pattern, especially of the third peak, they still could be significant sources of the solar *r*-elements of at least the second peak and lighter. If that is the case, heavier *r*-process elements must be synthesized in other sources. This is consistent with the scenario of multiple *r*-process sites implied by meteoritic abundances (Wasserburg, Busso, & Gallino 1996), spectroscopic studies of metal-poor halo stars (Sneden et al. 2000), and the chemical evolution studies (Ishimaru & Wanajo 2000). This could also be explained by the neutrino-driven wind models described here, which show the strong dependence of the *r*-process yields on the remnant mass.

In fact, most of the metal-poor stars in the Galactic halo show the higher ratios of light-to-heavy *r*-elements (e.g., Sr/Ba or Sr/Eu) than that of the solar *r*-abundances, although the values differ from star to star by up to ~ 2 orders of magnitude (McWilliam 1998; Ishimaru & Wanajo 2000). This implies that these *r*-elements might originate from the "weak" *r*-processing associated with smaller compaction ratios less than 0.28 (Figs. 4 and 5). However, some metal-poor stars (e.g., CS 22892-052) show somewhat smaller ratios of light-to-heavy *r*-elements compared to that of the solar *r*-abundances, by a factor of $\sim$ 2–3 (Sneden et al. 2000; see also Wasserburg et al. 1996 for a meteoritic study), which cannot be reproduced by any models in this study. If such low light-to-heavy ratios originate from neutrino-driven winds, we need somewhat more compact proto–neutron stars than considered in this study, otherwise we have to seek other causes to reduce the lighter *r*-nuclei, e.g., fallback of the first, low-entropy material ejected (Woosley et al. 1994).

Obviously, our approach of assuming constant values for the initial electron fraction, neutrino luminosity in each trajectory, the radius of the proto–neutron star, as well as an exponential time evolution of neutrino luminosity, is too simplified to conclude that these neutrino-driven wind models are an accurate description of the *r*-process. For example, the time variation of Y_e is of particular importance in the *r*-process. Recent hydrodynamic studies of core-collapse supernovae with accurate treatments of the neutrino transport have shown that Y_e exceeds 0.5 for the first few hundred milliseconds after core bounce (Rampp & Janka 2000). If that is the case, then the overproduction of $A \approx 90$ nuclei in our results would disappear (Hoffman et al. 1996). In the present study, the initial electron fraction was fixed at a relatively low value, 0.4, although it increases to 0.42–0.43 by the time of onset of the *r*-process. However, Y_e may be significantly higher than that during the early phase of the neutrino-driven wind. Even with a higher Y_e, however, a sufficient neutron-to-seed ratio could be obtained if the α-process is less efficient (Hoffman et al. 1997). Instead, the yields of *r*-process elements might decrease owing to a smaller amount of seed material.

Future hydrodynamic studies of core-collapse supernovae with accurate neutrino transport, including multidimensional effects such as convection and rotation, as well as magnetic fields, will probably ultimately be required before we can be certain that the neutrino-driven winds are indeed the major *r*-process site in the Galaxy. Nevertheless, our results have confirmed that the scenario of neutrino-driven winds is still viable and promising as the true astrophysical site for the *r*-process.

We would like to acknowledge useful discussions with Y. Ishimaru, N. Itoh, K. Sumiyoshi, and M. Terasawa. This work was supported in part by Japan Society for Promotion of Science, by the Grant in Aid for Scientific Research (1064236, 10044103, 11127220, and 12047233) of the Ministry of Education, Science, Sports and Culture of Japan, and by the Department of Energy Nuclear Theory grant DE-FG02-95-ER40394.

REFERENCES

Baumgarte, T. W., Janka, H.-Th., Keil, W., Shapiro, S. L., & Teukolsky, S. A. 1996, ApJ, 468, 823
Brown, G. W., & Bethe, H. A. 1994, ApJ, 423, 659
Cardall, C. Y., & Fuller, G. M. 1997, ApJ, 486, L111
Cowan, J., Thielemann, F.-K., & Truran, J. W. 1991, Phys. Rep., 208, 267
Freiburghaus, C., Rembges, J.-F., Rauscher, T., Kolbe, E., Thielemann, F.-K., Kratz, K.-L., Pfeiffer, B., & Cowan, J. J. 1999, ApJ, 516, 381
Freiburghaus, C., Rosswog, S., & Thielemann, F.-K. 1999, ApJ, 525, L121
Glendenning, N. K. 1985, ApJ, 293, 470
———. 1989, Nucl. Phys. A, 493, 521
Glendenning, N. K., & Weber, F. 1992, ApJ, 400, 647
Hoffman, R. D., Woosley, S. E., Fuller, G. M., & Meyer, B. S. 1996, ApJ, 460, 478
Hoffman, R. D., Woosley, S. E., & Qian, Y.-Z. 1997, ApJ, 482, 951
Ishimaru, Y., & Wanajo, S. 1999, ApJ, 511, L33
———. 2000, in First Stars, ed. A. Weiss, T. Abel, & V. Hill (Berlin: Springer), 189
Itoh, N., Hayashi, H., Nishikawa, A., & Kohyama, Y. 1996, ApJS, 102, 411
Käppeler, F., Beer, H., & Wisshak, K. 1989, Rep. Prog. Phys., 52, 945
Keil, W., & Janka, H.-Th. 1995, A&A, 296, 145
McWilliam, A. 1997, ARA&A, 35, 503
———. 1998, AJ, 115, 1640
Meyer, B. S., Mathews, G. J., Howard, W. M., Woosley, S. E., & Hoffman, R. D. 1992, ApJ, 399, 656
Meyer, B. S., McLaughlin, G. C., & Fuller, G. M. 1998, Phys. Rev. C, 58, 3696
Otsuki, K., Tagoshi, H., Kajino, T., & Wanajo, S. 2000, ApJ, 533, 424 (Paper I)
Qian, Y.-Z. 2000, ApJ, 534, L67
Qian, Y.-Z., Vogel, P., & Wasserburg, G. J. 1998, ApJ, 494, 285
Qian, Y.-Z., & Woosley, S. E. 1996, ApJ, 471, 331
Rampp, M., & Janka, H.-Th. 2000, ApJ, 539, L33
Ryan, S. G., Norris, J. E., & Beers, T. C. 1996, ApJ, 471, 254
Shapiro, P., & Teukolsky, S. 1983, Black Holes, White Dwarfs, and Neutron Stars (New York: Wiley)
Sneden, C., Cowan, J. J., Debra, L. B., & Truran, J. W. 1998, ApJ, 496, 235
Sneden, C., Cowan, J. J., Ivans, I. I., Fuller, G. M., Burles, S., Beers, T. C., & Lawler, J. E. 2000, ApJ, 533, L139
Sneden, C., McWilliam, A., Preston, G. W., Cowan, J. J., Burris, D. L., & Armosky, B. J. 1996, ApJ, 467, 819
Sumiyoshi, K., Suzuki, H., Otsuki, K., Terasawa, M., & Yamada, S. 2000, PASJ, 52, 601
Takahashi, K., Witti, J., & Janka, H.-Th. 1994, A&A, 286, 857
Thorsson, V., Prakash, M., & Lattimer, J. M. 1994, Nucl. Phys. A, 572, 693
Tsujimoto, T., Shigeyama, T., & Yoshii, Y. 2000, ApJ, 531, L33
Wasserburg, G. J., Busso, M., & Gallino, R. 1996, ApJ, 466, L109
Weber, F., & Weigel, M. K. 1989, Nucl. Phys. A, 505, 779
Wheeler, J. C., Cowan, J. J., & Hillebrandt, W. 1998, ApJ, 493, L101
Wiringa, R. B., Fiks, U., & Fabrocini, A. 1988, Phys. Rev. C, 38, 1010
Witti, J., Janka, H.-Th., & Takahashi, K. 1994, A&A, 286, 841
Woosley, S. E., & Hoffman, R. D. 1992, ApJ, 395, 202
Woosley, S. E., Wilson, J. R., Mathews, G. J., Hoffman, R. D., & Meyer, B. S. 1994, ApJ, 433, 229